

Part IV - Ch 5 Performance of ports and waterway systems

van Koningsveld, M.; van der Werff, S.E.; Jiang, M.; Lansen, A.J.; de Vriend, H.J.

Publication date

2021

Document Version

Final published version

Published in

Ports and Waterways

Citation (APA)

van Koningsveld, M., van der Werff, S. E., Jiang, M., Lansen, A. J., & de Vriend, H. J. (2021). Part IV - Ch 5 Performance of ports and waterway systems. In M. V. Koningsveld, H. J. Verheij, P. Taneja, & H. J. de Vriend (Eds.), *Ports and Waterways: Navigating a changing world* (pp. 433-458). TU Delft OPEN Publishing.

Important note

To cite this publication, please use the final published version (if applicable).
Please check the document version above.

Copyright

Other than for strictly personal use, it is not permitted to download, forward or distribute the text or part of it, without the consent of the author(s) and/or copyright holder(s), unless the work is under an open content license such as Creative Commons.

Takedown policy

Please contact us and provide details if you believe this document breaches copyrights.
We will remove access to the work immediately and investigate your claim.

5 Performance of port and waterway systems

5.1 Energy consumption and emissions by IWT vessels

In [Part I – Section 2.1.1](#) the emerging energy transition was discussed as an important trigger of change. It should be regarded in the context of the 2015 Paris Agreement: the first universal, legally binding climate agreement. It aims to limit global warming, and one of the key elements is to reduce emissions worldwide ([European Commission, 2021](#)). As a contribution to this agreement, participating countries had to deliver national climate action plans. The aforementioned [IMO](#) restrictions to the sulphur and nitrogen content of fuel are an international example. In 2019, the Netherlands established their national climate agreement with ambitious emission reduction goals ([Min. EZK, 2019](#)).

Following these developments, various economic sectors are pressed to reduce emissions, also the [IWT](#) sector. To respond to this pressure a Green Deal has been agreed to by [IWT](#) stakeholders ([Green Deal, 2019](#)). It defines goals and ambitions for inland shipping for the upcoming years, concerning CO₂- and environmental pollutant emissions. concerning the CO₂ emissions and emissions of environmental pollutants. The main aims and objectives are (see also [Figure 5.1](#)).

- 2024 – A reduction of CO₂ emissions of at least 20% compared to 2015, and a reduction of environmental pollutants of at least 10% compared to 2015.
- 2030 – A reduction of CO₂ emissions of 40% to 50% compared to 2015;
- 2035 – A reduction of environmental pollutants of 35% to 50% compared to 2015;
- 2050 – Emission-free and climate-neutral inland shipping achieved.

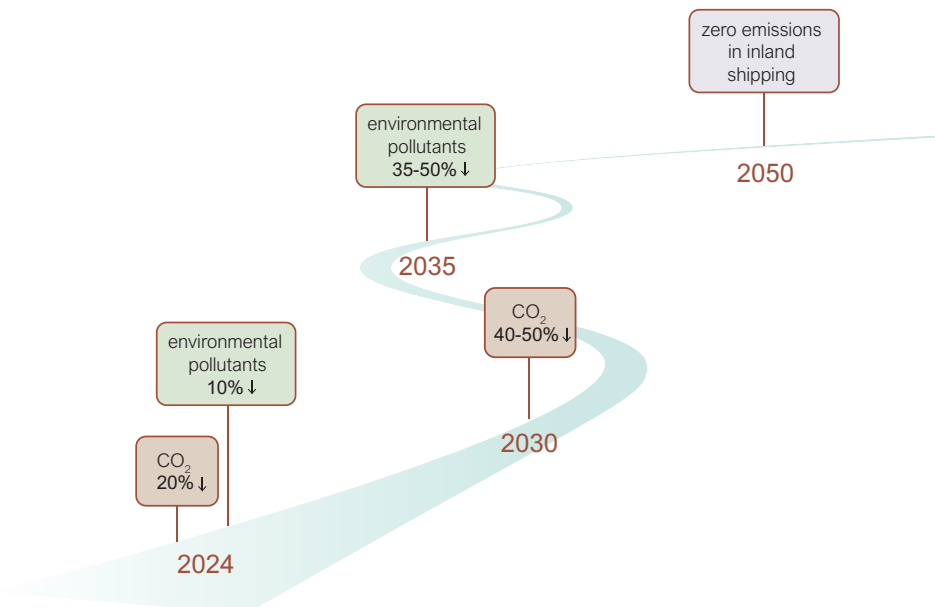


Figure 5.1: Time line Green Deal – goals and ambitions for inland shipping (image modified from [Segers, 2021](#), by TU Delft – Ports and Waterways is licenced under CC BY-NC-SA 4.0).

To meet these goals numerous task groups and studies have been initiated to investigate which alternative energy carriers are most promising, what requirements these energy carriers pose for the bunkering infrastructure and what packages of policy measures are likely to be most effective. For each of these and many other similar questions a detailed insight into the current and potential future energy consumption and associated emissions is crucial.

According to CBS (2021b) the total Dutch transport sector was responsible for approximately 12% of all Greenhouse Gas (GHG) emission by the Dutch economy. Within the transport sector 45% of emissions is caused by aviation, 30% by transport over water (sea and inland shipping) and 21% by road transport. The remaining 4% is attributed to transport related services. Two thirds of those emissions take place outside the Netherlands, viz. international aviation and shipping. According to CBS (2021a) IWT inside the Netherlands emitted in 2019 1.94 mln kg CO₂, 25.3 mln kg NO_x and 0.82 mln kg PM10.

To facilitate rational decision making more insight in emission sources is needed than is provided by the aggregated figures discussed above. Various methods to estimate the energy consumption and the associated emissions of an individual IWT-vessel have already been published, i.e. Bolt (2003); Hekkenberg (2012); Vehmeijer (2019); Rijkswaterstaat (2021) and many more.

What all methods including the one described below have in common is that they start with estimating the resistance a vessel experiences when sailing at a given speed. The older methods rely on more simple vessel resistance equations and hydrodynamic effects around the vessels. See Part III – Section 4.5. The estimated resistance is translated to engine power requirements through a number of empirical loss factors. This required engine power can then be used to estimate the required energy for a given time interval. Based on empirical data one can estimate the amount of fuel that is needed to deliver this energy. Depending on the selected fuel type and some additional information such as installed power and engine age an estimate can be made of associated potential for emission. NB: the addition of ‘potential’ is important to notice, since on-board measures may be implemented to scrub or filter out these emissions before they are in actually emitted, albeit to additional cost.

Below we describe a methodology that is largely in line with the common practice to estimate energy consumption and emissions, with the particular addition that energy consumption and emissions for an individual vessel will be calculated and logged as a function of time and space. Furthermore we add empirical relations to translate the estimated energy consumption to emissions of interest, viz. CO₂, NO_x and PM10. These are useful additions when one is interested in network performance, and to adhere to current QSCs and reference values or targets. By applying the methodology to a representative selection of vessels making representative trips on the transport network, it becomes possible to make bottom-up estimates of energy consumption and emission patterns. This in turn allows for the inter-comparison of policy measures and investment strategies.

Figure 5.2 describes the components of the methodology we will discuss. The method is based on work by Segers (2021). Starting point of the analysis are the ship dimensions (length (L_s), beam (B_s) and draught (D_s)), the sailing speed of the vessel (V_s), and the waterway characteristics (water depth (h_0), ambient current (U_c)). With this information we can estimate the total resistance (kN) a vessel experiences while sailing at a given velocity with respect to the water.

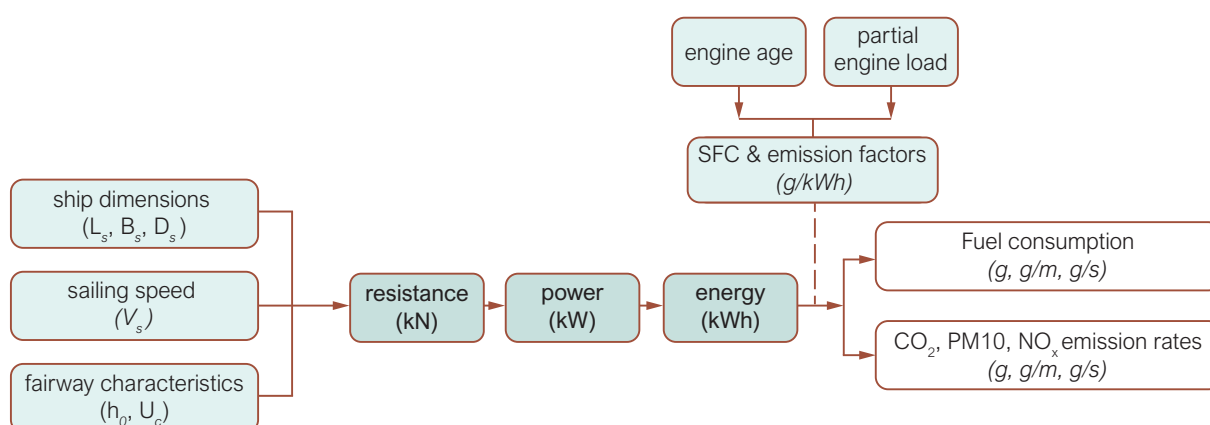


Figure 5.2: Methodology for estimating emissions for IWT vessels (image modified from Segers, 2021, by TU Delft – Ports and Waterways is licenced under CC BY-NC-SA 4.0).

Once the total resistance (kN) is calculated we estimate the power (kW) that is required to overcome this resistance. We provide estimates of the Effective Horse Power (EHP), the Delivered Horse Power (DHP) and ultimately the Brake Horse Power (BHP) by applying a number of efficiency factors. The total required power can further be subdivided into the power required for propulsion and the power needed for hotel systems on board.

Once the total required power is ‘known’ we can calculate the energy (kWh) that is consumed by multiplying the total power with the duration of its application. The energy consumption estimate can then be translated to emissions based on empirical relations between energy use and fuel consumption, and fuel consumption and emissions.

Below we treat each substep briefly. For more detail we refer to [Segers \(2021\)](#).

5.1.1 Resistance

For the calculation of the total resistance (R_T) a vessel experiences we use the approach suggested by [Holtrop and Mennen \(1982\)](#). They estimate the total resistance, R_T , from a range of components.

$$R_T = R_f(1 + k_1) + R_w + R_{app} + R_{res} \quad (5.1)$$

In which:

R_T	=	total resistance of the ship [kN],
R_f	=	frictional resistance [kN],
$1 + k_1$	=	form factor of the hull [-],
R_w	=	wave resistance [kN], and
R_{app}	=	appendage resistance [kN],
R_{res}	=	residual resistance [kN].

Frictional resistance including the hull form factor: $R_f(1 + k_1)$

The general way to calculate the drag of an object is by multiplying the dynamic pressure of the fluid by a dimensionless drag coefficient and a surface area. As we have seen in [Part III – Section 4.5](#), the frictional resistance of a vessel follows from

$$R_f = \frac{1}{2} \rho_w V_s^2 \cdot C_f \cdot S \quad (5.2)$$

in which:

$\frac{1}{2} \rho_w V_s^2$	=	dynamic pressure of the fluid [N/m^2],
C_f	=	friction coefficient [-], and
S	=	wetted surface area of the hull [m^2].

As the frictional resistance constitutes a large part of the total resistance, it makes sense to approximate the friction coefficient and the wetted surface area as accurately as possible.

In deep water ($h_0/L_s > 1$), the friction coefficient for a body with a smooth flat bottom and no friction on the sides depends only on the Reynolds number. [Zeng et al. \(2018\)](#) derive on the basis of CFD-model computations:

$$C_{f, \text{deep}} = \frac{0.08169}{(\log Re - 1.717)^2} \quad (5.3)$$

in which $Re = V_s L_s / \nu$, with ν the kinematic viscosity [m^2/s] ($\approx 1 \cdot 10^{-6}$). In shallow water ($h_0/L_s < 1$), however, other parameters come into play. Again on the basis of CFD-model computations [Zeng et al. \(2018\)](#) derive:

$$C_{f, \text{shallow}} = \frac{0.08169}{(\log Re - 1.717)^2} \left[1 + \frac{0.003998}{\log Re - 4.393} \left(\frac{h_0 - z - D_s}{L_s} \right)^{-1.083} \right] \quad (5.4)$$

in which h_0 is the undisturbed water depth, z is the maximum water level depression and D_s is the draught of the ship. When taking the friction at the submerged flanks of the ship into account, this becomes:

$$C_f = C_{f_0} + (C_{f, \text{shallow}} - C_{f, \text{Katsui}}) \frac{S_B}{S} \left(\frac{V_s + \Delta V}{V_s} \right)^2 \quad (5.5)$$

In which:

- C_{f_0} = frictional resistance according to the ITTC-1957 curve [-]; see [Equation 5.6](#),
- $C_{f, \text{Katsui}}$ = Katsui's friction coefficient for a flat plate in unrestricted water [-]; see [Equation 5.7](#),
- S_B = area of the flat bottom [m^2],
- V_s = relative free stream velocity [m/s], or the ships speed (V'_s in case of ambient current), and
- $V_s + \Delta V$ = velocity underneath ship's bottom [m/s] ($V'_s + \Delta V$ in case of ambient current); see [Equation 5.11](#) and [Equation 5.14](#).

Following in-depth discussions the [ITTC \(1957\)](#) agreed on the following frictional resistance curve ([ITTC, 2002](#)):

$$C_{f_0} = \frac{0.075}{(\log Re - 2)^2} \quad (5.6)$$

[Katsui et al. \(2005\)](#) proposed a friction coefficient for a smooth flat plate in deep water:

$$C_{f, \text{Katsui}} = \frac{0.0066577}{(\log Re - 4.3762)^a} \quad (5.7)$$

where $a = 0.042612 \log Re + 0.56725$.

The area of the flat bottom, S_B , is estimated by taking $L_s \cdot B_s$. For the wetted surface area of the hull [Holtrop and Mennen \(1982\)](#) give the following empirical formula:

$$S = L_s(2D_s + B_s) \sqrt{C_M} \left[0.453 + 0.4425C_B - 0.2862C_M - 0.003467 \frac{B_s}{D_s} + 0.3696C_{WP} \right] + 2.38 \frac{A_{BT}}{C_B} \quad (5.8)$$

In which:

- L_s = the ship's length [m] at the waterline,
- D_s = draught [m],
- B_s = beam [m],
- C_M = midship section coefficient [-],
- C_B = block coefficient [-] on the basis of the waterline length,
- C_{WP} = water plane area coefficient [-], and
- A_{BT} = cross-sectional area of the bulb at still water level [m^2].

The block coefficient is relatively high for inland vessels. For now we assume it to be constant at 0.85; this is the maximum value for which the method of [Holtrop and Mennen \(1982\)](#) is still applicable. Furthermore, most inland ships do not have a bulb. So we assume $A_{BT} = 0$.

[Bertram and Schneekluth \(1998\)](#) relate both C_M and C_{WP} to the block coefficient:

$$C_M = 1.006 - 0.0056C_B^{-3.56} \quad (5.9)$$

$$C_{WP} = \frac{1 + 2C_B}{3} \quad (5.10)$$

The velocity underneath the ship's bottom, $V_s + \Delta V$, according to [Zeng et al. \(2018\)](#) can be estimated with:

$$V_s + \Delta V = 0.4277 \cdot V_s \cdot \exp\left(\frac{h_0}{D_s}\right)^{-0.07634} \quad (5.11)$$

The uncertainty of this formula is 2.5% and it is only suitable for $h_0/D_s \leq 4.0$. When $h_0/D_s > 4.0$, $V_s + \Delta V$ is assumed to be equal to V_s . Note that for resistance calculations $V_s + U_r$ according to [Schijf \(1949\)](#) is typically thought too coarse. The value of $V_s + \Delta V$ refers to the actual velocities directly underneath the vessel, which are higher than the cross-section averaged values that follow from [Schijf \(1949\)](#).

Other than [Holtrop and Mennen \(1982\)](#), we use the method proposed by [Watson \(1998\)](#) to calculate the hull form factor $(1 + k_1)$:

$$1 + k_1 = 0.93 + 0.487c_{14} \left(\frac{B_s}{L_s}\right)^{1.068} \left(\frac{D_s}{L_s}\right)^{0.461} \left(\frac{L_s}{L_R}\right)^{0.122} \left(\frac{L^3}{\nabla}\right)^{0.365} (1 - C_P)^{-0.604} \quad (5.12)$$

In which:

- c_{14} = coefficient accounting for the specific shape of the ship's afterbody, here assumed to be 1 [-],
- L_R = length parameter [m],
- ∇ = the ship's water displacement [m^3], $C_B \cdot L_s \cdot B_s \cdot D_s$, and
- C_P = C_B/C_M = the so-called prismatic coefficient [-].

According to [Holtrop and Mennen \(1982\)](#) the length parameter L_R can be calculated from:

$$L_R = L_s \left[1 - C_P + \frac{0.06C_P}{4C_P - 1} (19.4C_P - 13.5) \right] \quad (5.13)$$

With these values the hull form factor, $1 + k_1$, can be determined using [Equation 5.12](#), and with it the effect of viscosity on the frictional resistance ([Equation 5.2](#)).

Note that for now we assume $C_B = 0.85$, $c_{14} = 1$ and $A_{BT} = 0$.

Wave resistance: R_w

We used [Equation 5.11](#) to estimate the accelerated velocity underneath the ship's bottom to account for shallow water effects in the calculation of friction resistance, R_f . Likewise, limited water depth also has a significant influence on the wave resistance, R_w .

When a vessel starts to approach its critical speed, V_{lim} , the wave resistance increases significantly. Although Schijf's method (see also [Part III – Chapter 4](#)) corrects for the channel cross-section, it does not correct for shallow water effects on the currents directly underneath the vessel ([Hekkenberg, 2012](#)). [Segers \(2021\)](#) implements the Karpov method ([Van Terwisga, 1989](#)) to estimate this velocity increase. The velocity underneath the ship's bottom, $V_s + \Delta V$, for wave resistance can be calculated with:

$$V_s + \Delta V = \frac{V_s}{\alpha^{**}} \quad (5.14)$$

Coefficient α^{**} depends on Fr_h , the Froude number based on the ship's speed and water depth:

$$Fr_h = \frac{V_s}{\sqrt{gh_0}} \quad (5.15)$$

Figure 5.3 shows the estimation of α^{**} based on the Froude number Fr_h for different h_0/D_s ratios. The appropriate value of α^{**} can thus be selected to derive $V_s + \Delta V$ using Equation 5.14. $V_s + \Delta V$ from Equation 5.14 can be used in the wave resistance calculations but also for the other remaining resistance components.

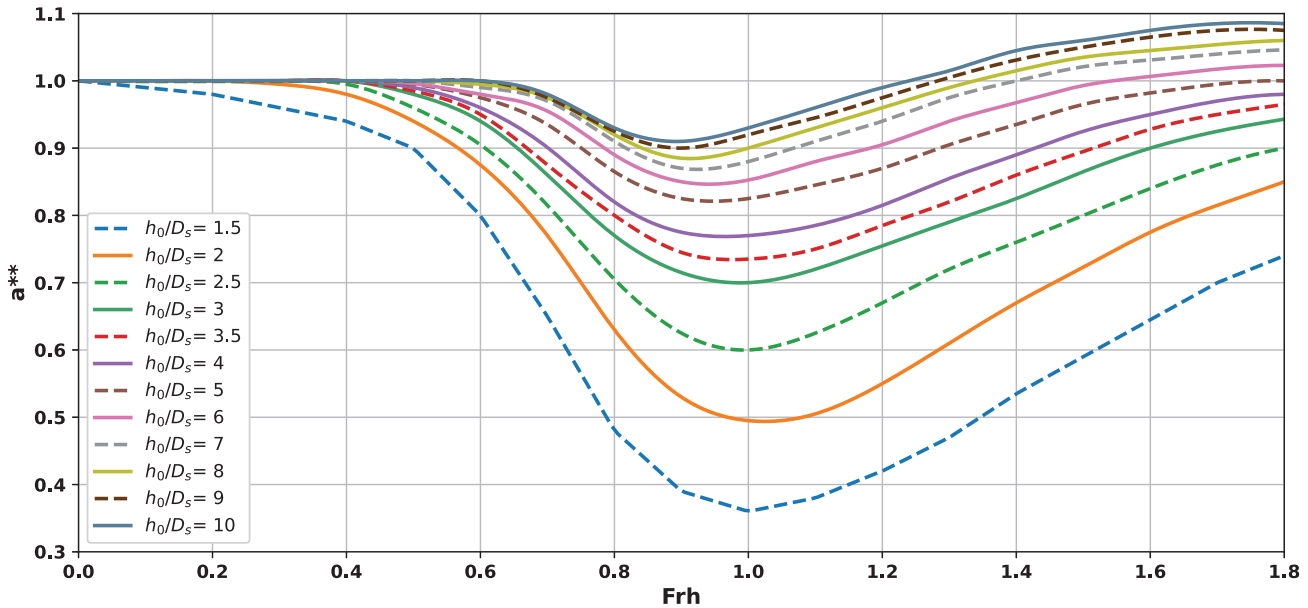


Figure 5.3: Karpov method: estimation of α^{**} based on the Froude number Fr_h for different h_0/D_s ratios (image modified from Segers, 2021, by TU Delft – Ports and Waterways is licenced under CC BY-NC-SA 4.0).

Holtrop and Mennen (1982) express the wave resistance as

$$R_w = c_1 c_2 c_5 \rho_w g \nabla \exp \left(m_1 Fr_L^d + m_2 \cos(\lambda Fr_L^{-2}) \right) \quad (5.16)$$

in which:

- Fr_L = the Froude number based on the ship's speed relative to the water and its length,
- c_1 = an empirical coefficient of proportionality [-],
- c_2 = an empirical coefficient accounting for the reducing effect of the bulbous bow on the wave resistance [-],
- c_5 = an empirical coefficient accounting for the effect of the transom stern (i.e. a flat stern extending to the water line) on the wave resistance [-], and
- m_1, m_2, d and λ are empirical parameters.

These quantities can be evaluated according to the rules in Table 5.1, in which

- A_T = area of the immersed part of the transom stern at zero speed, assumed to be $0.1 \cdot B_s \cdot D_s$,
- i_E = angle of the waterline at the bow with respect to the central plane,
- $D_{s,bow}$ = draught at the front of the bow, and
- h_B = position of the centre of the bulb cross-section at the waterline above the keel line, approximately equal to $D_s/2$.

Appendage resistance: R_{app}

The appendages of a ship, such as the rudder, the skeg and the shaft, cause extra resistance, mainly frictional. As the contribution of these terms is relatively small, we will not further elaborate them here. We refer to (Segers, 2021) for further detail.

Quantity	Formula	Condition
c_1	$2223105c_7^{3.78613}(D_s/B_s)^{1.07961}(90 - i_E)^{-1.37565}$	
c_7	$0.229577(B_s/L_s)^{0.33333}$ B_s/L_s $0.5 - 0.0625L_s/B_s$	$B_s/L_s < 0.11$ $0.11 \leq B_s/L_s \leq 0.25$ $B_s/L_s > 0.25$
i_E	$1 + 89 \exp\left(-\left(\frac{L_s}{B_s}\right)^{0.80856} (1 - C_{WP})^{0.30484} \dots\right.$ $\left.\dots (1 - C_p - 0.0225 \cdot lcb)^{0.6367} \left(\frac{L_R}{B_s}\right)^{0.34574} \left(\frac{100\nabla}{L_s^3}\right)^{0.16302}\right)$	
lcb	$19.4C_p - 13.5$	
c_2	$\exp(-1.89\sqrt{c_3})$	
c_3	$0.56A_{BT}^{1.5} / [B_s D_s (0.31\sqrt{A_{BT}} + D_{s,bow} - h_B)]$	
c_5	$1 - 0.8A_T / (B_s D_s C_M)$	
λ	$1.446C_p - 0.03L_s/B_s$ $1.446C_p - 0.36$	$L_s/B_s < 12$ $L_s/B_s \geq 12$
m_1	$0.0140407\frac{L_s}{D_s} - 1.75254\frac{\nabla^{1/3}}{L_s} - 4.79323\frac{B_s}{L_s} - c_{16}$	
c_{16}	$8.07981C_p - 13.8673C_p^2 + 6.984388C_p^3$ $1.73014 - 0.7067C_p$	$C_p < 0.80$ $C_p \geq 0.80$
m_2	$c_{15}C_p^2 \exp(-0.1Fr_L^{-2})$	
c_{15}	-1.69385 $-1.69385 + \left(\frac{L_s}{\nabla^{1/3}} - 8.0\right) / 2.36$ 0	$L_s^3/\nabla < 512$ $512 \leq L_s^3/\nabla \leq 1727$ $L_s^3/\nabla > 1727$
d	-0.9	

Table 5.1: Evaluation of wave resistance parameters (Holtrop and Mennen, 1982).

Residual resistance terms

The residual resistance components are due to the immersed parts of the bulbous bow and the transom stern, and the effect of the hull-roughness and the still-air resistance. The formulations to estimate them, as suggested by Holtrop and Mennen (1982), are of a similar form as the formulation of the frictional resistance, viz. dynamic pressure of the fluid times a friction coefficient times a surface formulation. The cumulative contribution of the residual friction terms can be considerable, but is typically much smaller than the frictional resistance. Since these terms follow the same formulation as the frictional resistance their behaviour is also similar. For further detail on the quantification of this term the reader is referred to Segers (2021).

Relative importance of the resistance terms

In order to get an impression of the relative importance of the various resistance terms, the total resistance and its components have been calculated for an inland vessel according to RWS Class M9 of dimensions $135 \times 11.45 \times 2.75$ m, sailing in water of 10 m depth. Figure 5.4 gives the results as a function of the relative speed. It shows that at higher speeds the wave effects and friction are the major resistance components.

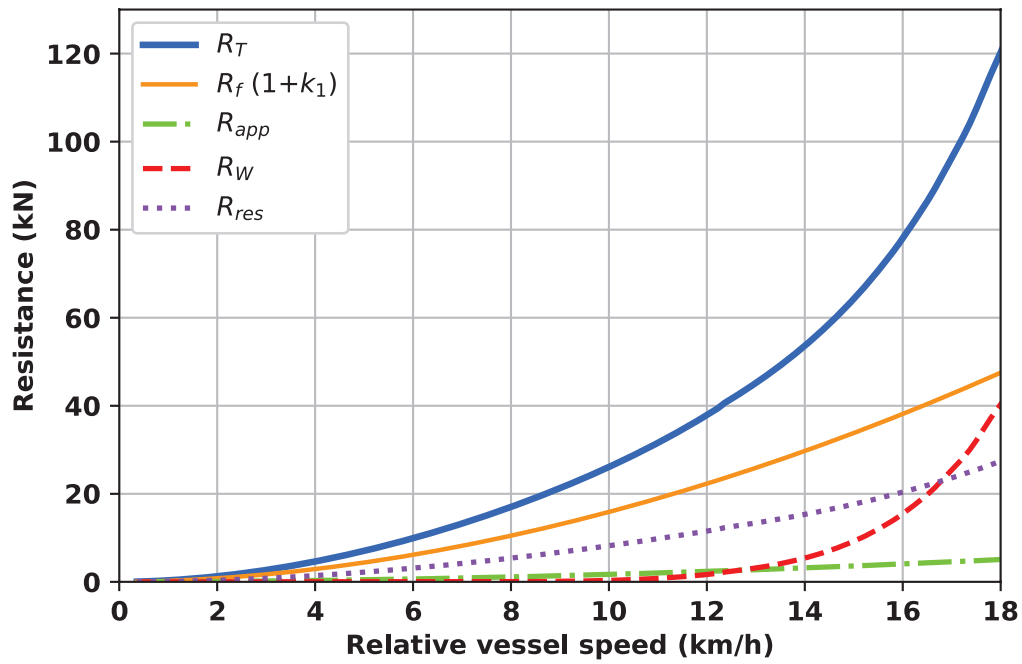


Figure 5.4: Resistance components as a function of the relative vessel speed ($h_0 = 7.5$ m) (image modified from Segers, 2021, by TU Delft – Ports and Waterways is licenced under CC BY-NC-SA 4.0).

In shallow water the resistance is a function of the water depth. Figure 5.5 shows the total resistance, R_T , for the same ship as above, but now for different water depths. The figure clearly shows the depth-dependence with the total resistance drastically increasing for higher velocities at lower water depths.

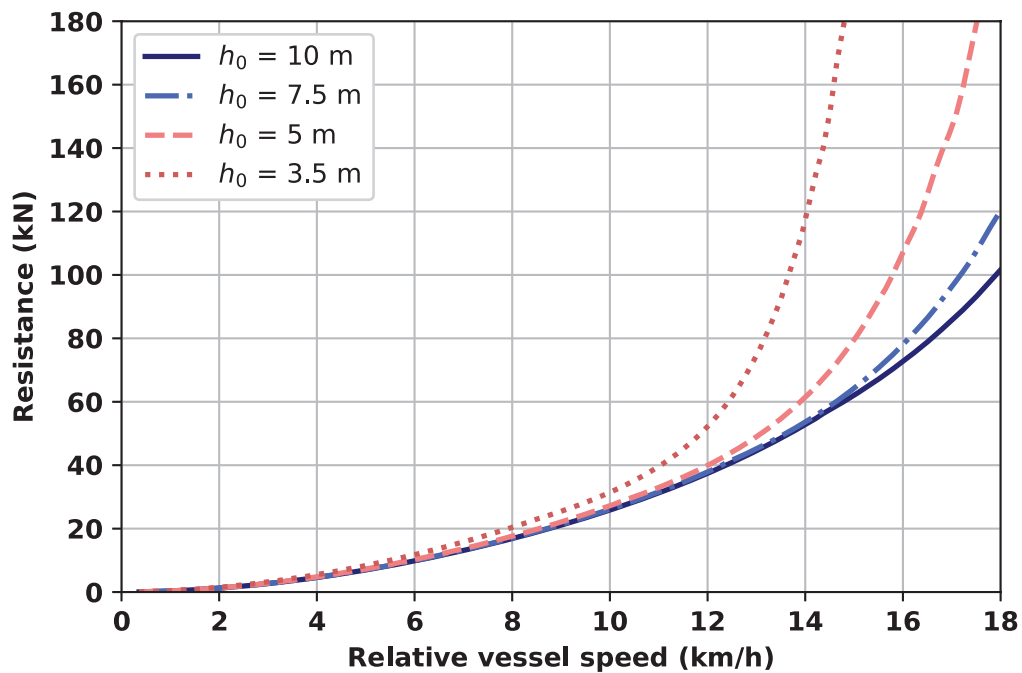


Figure 5.5: Total resistance as a function of the relative vessel speed, for different water depths (image modified from Segers, 2021, by TU Delft – Ports and Waterways is licenced under CC BY-NC-SA 4.0).

5.1.2 Power

The previous subsection outlines an approach to quantify the total resistance of a vessel with the ship’s dimensions (L_s , B_s and D_s), sailing speed (V_s) and fairway characteristics (h_0 and U_c) as inputs. The next step in the methodology (Figure 5.2) is to estimate the power that is needed to overcome this resistance.

Starting point for this step is the **Effective Horse Power (EHP)** requirement, which is the work done by the moving vessel. It follows from:

$$P_e = V_s R_T \quad (5.17)$$

In which:

- P_e = effective power [kW],
- V_s = ship speed relative to the water [m/s], and
- R_T = total resistance [kN].

Equation 5.17 can be evaluated now that R_T is known. Since P_e is directly related to the total resistance, R_T , it straightforwardly follows from Figure 5.4 that the required power rapidly increases when a vessel sails faster in the same water depth, and from Figure 5.5 that it rapidly increases when a vessel aims to maintain the same speed as the water gets shallower and the underkeel clearance decreases. The effective power requirement is an important input when designing a ship's power system.

A ship designer has various options for the power generation and distribution system: mechanical, diesel-electric, or a combination of these. Figure 5.6 schematically represents these alternatives. In the mechanical system the **Main Propulsion Engine (MPE)** is connected to the propeller via a shaft. In the case of a four-stroke engine, which operates at a higher frequency than a two-stroke one, a gear box is required. An additional advantage of such a gear box is that it can couple more than one engine to the shaft. Apart from the **MPE**, there can be diesel-electric generators on board to generate the power needed for the electric systems on board, the so-called hotel power. Part of the electricity produced can be diverted to the propulsion system through a **Power-Take-In (PTI)** system. On the other hand, part of the mechanical power produced by the **MPE** can be diverted to the hotel power through a **Power-Take-Off (PTO)** system. These facilities enable optimising the power generation system on board. Baldasso et al. (2019) describe a method to do so.

For cargo vessels the hotel power amounts on average to some 8% of the installed power. The other 92% is available for propulsion, but not all power that is generated by the engine is effective due to losses in the transmission system. Figure 5.7 schematically shows such a system for a four-stroke **MPE** with gearbox in propulsion mode.

The engine power available for propulsion is transferred to the propeller via a transmission system consisting of a gearbox and a shaft with bearings. The energy losses they cause are usually expressed in terms of efficiency

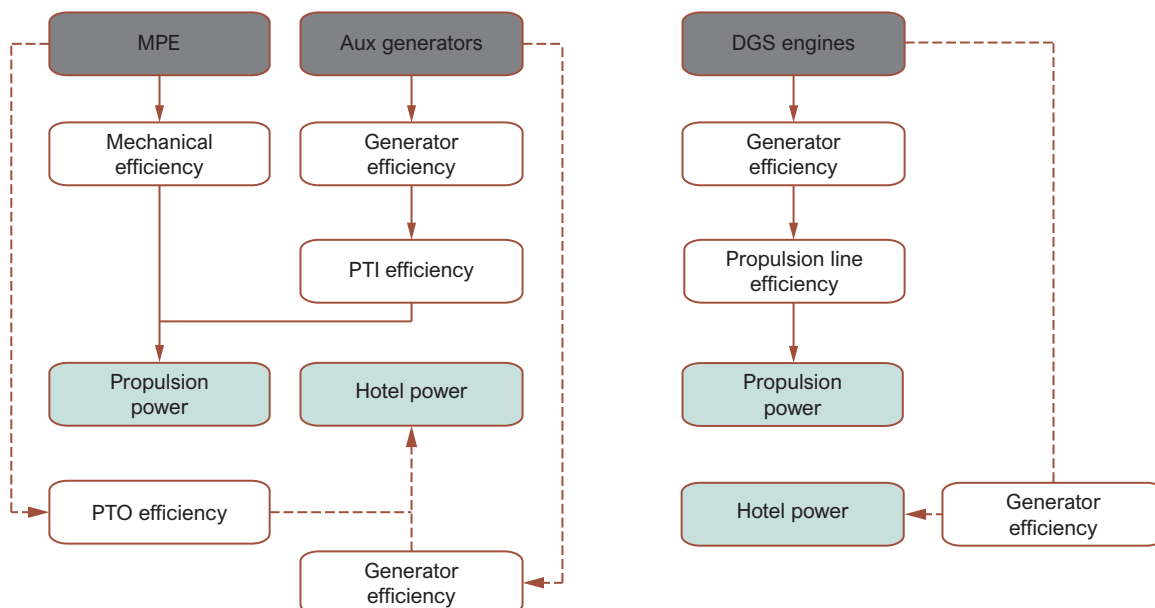


Figure 5.6: Power generation alternatives, left: mechanical system; right: diesel-electric system (image reworked from Baldasso et al., 2019, by TU Delft – Ports and Waterways is licenced under CC BY-NC-SA 4.0.).

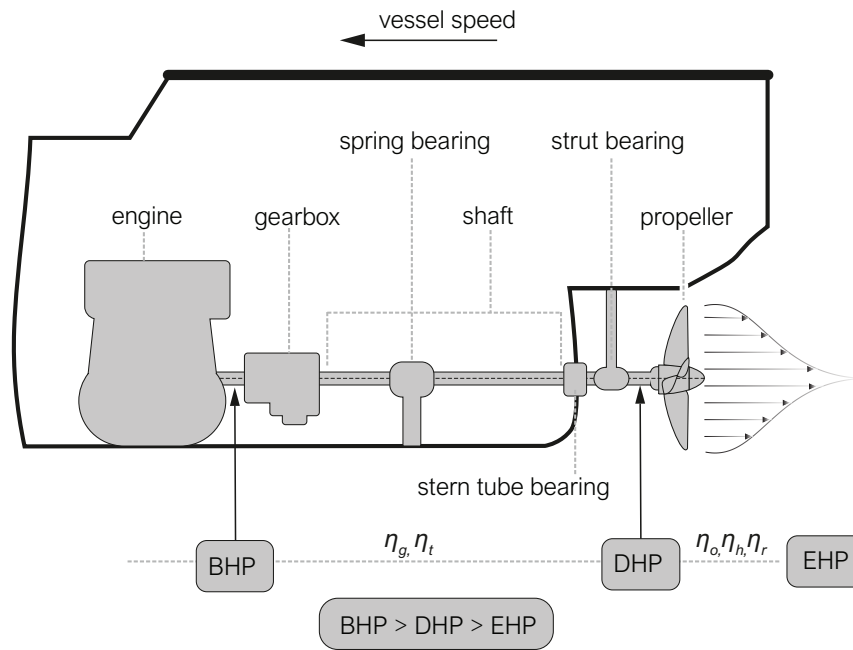


Figure 5.7: Schematization of a ship in propulsion mode, illustrating different power components and efficiencies (image modified from Segers, 2021, by TU Delft – Ports and Waterways is licenced under CC BY-NC-SA 4.0).

factors in the relationship between the power for propulsion (Brake Horse Power (BHP)) and the power actually delivered to the propeller (Delivered Horse Power (DHP)):

$$P_d = \eta_g \eta_t P_b \tag{5.18}$$

In which:

- P_d = delivered horse power [kW],
- P_b = brake horse power [kW],
- η_g = gearing efficiency [-], and
- η_t = transmission efficiency [-].

Commonly used values are 0.96 for the gearing efficiency and 0.98 for the transmission efficiency.

Between the DHP and the EHP that is really available for propulsion there are efficiency losses associated with the hull and the propeller. Hence:

$$P_e = \eta_o \eta_r \eta_h P_d \tag{5.19}$$

In which:

- P_e = effective horse power [kW],
- η_o = open water efficiency of the propeller [-],
- η_r = relative rotative efficiency of the propeller [-], and
- η_h = hull efficiency [-].

The *open water efficiency* of the propeller is the ratio of the thrust power produced by the propeller and the power absorbed by it in open water, i.e. if there is no hull in front of it. Its value depends on the speed of advance and the propeller design and dimensions. Typical values are between 0.55 and 0.70.

The *relative rotative efficiency* of the propeller accounts for the variation in water flow to the propeller in the wake behind the ship, as compared with the open water flow conditions. The value of the efficiency factor generally lies close to one (0.98 - 1.02).

The *hull efficiency* is determined with the following formula

$$\eta_h = \frac{1 - t}{1 - w} \quad (5.20)$$

In which:

$$\begin{aligned} t &= \text{thrust deduction factor [-]}, \\ w &= \text{wake fraction [-]} \end{aligned}$$

The relative speed of advance of a ship's propeller, V_A , is generally smaller than the speed of the vessel relative to the water, V_s . This effect, which is due to the wake behind the ship, is expressed in the wake fraction coefficient:

$$w = (V_s - V_A)/V_s \quad (5.21)$$

The value of w depends on the shape of the hull, but also on size and location of the propeller. Ships with a large block coefficient have a large wake fraction coefficient, and the water motion around the propeller is very inhomogeneous. For ships with a single propeller, the coefficient lies normally between 0.20 and 0.45. Segers (2021) describes a method to calculate this coefficient, based on an empirical method of Pappel described by Van Terwisga (1989).

The thrust deduction factor is a function of w . In case of a single-screw vessel it reads

$$t = 0.6w(1 + 0.67w) \quad (5.22)$$

for a double-screw vessel:

$$t = 0.8w(1 + 0.25w) \quad (5.23)$$

Equation 5.17, Equation 5.18 and Equation 5.19 and their efficiency factors, reason from the propulsion power towards the effective power. For our methodology we use these equations the other way around to estimate the required engine power for propulsion (BHP) with R_T as a starting point:

$$P_{\text{propulsion}} = P_b = V_s R_T \cdot \frac{1}{\eta_0 \eta_r \eta_h} \cdot \frac{1}{\eta_g \eta_t} \quad (5.24)$$

Beside the propulsion power, there are many other power-consuming systems on board. In order to estimate the hotel power requirements, one may use a load chart (Marine Insight, 2020). Such a chart distinguishes three situations: sailing, manoeuvring and harbour (see Table 5.2 for an example). The power requirements of each electrical system on board is calculated by multiplying the so-called **Maximum Rated Power (MRP)**, i.e. the maximum power the specific device can have, by two factors, viz.

- the load factor LF , which is the ratio of the operational power and the **MRP**, and
- the utility factor UF , which indicates to what extent the device is used in a particular situation.

In combination with the electrical power needed for propulsion (in case of a diesel-electric engine system) this leads to total generator capacity required.

When vessels become larger, the hotel power component increases. For modern cruise ships, for example, the hotel power may amount to 40% of the total installed power. For **IWT**-vessels, however, the hotel component is

Device	# inst.	# in use	MRP (kW)	Pinst (kW)	Sailing			Manoeuvring			Harbour		
					LF	UF	kW	LF	UF	kW	LF	UF	kW
Steering gear	2	1	24	27	0.8	0.8	17	0.8	0.8	17	0.8	0	0
Windlass	1	1	37	41	0.8	0	0	0.8	0.7	23	0.8	0	0
Baggage crane	2	1	14	16	0.8	0	0	0.8	0	0	0.8	0.6	7.5
Mooring winch	2	1	20	22	0.8	0	0	0.8	0.7	12	0.8	0	0
ER-crane	1	1	4	5	0.8	0.1	0.4	0.8	0	0	0.8	0.2	0.8
Provision davit	2	2	5	6	0.8	0.1	0.9	0.8	0.1	0.9	0.8	0.5	4.7
Galley equipmt	1	1	489	544	0.8	0.2	87	0.8	0.2	87	0.8	0.1	44
Laundry equipmt	1	1	85	95	0.8	0.2	15	0.8	0.2	15	0.8	0	0
Ventilation	1	1	110	122	0.8	0.8	78	0.8	0.8	78	0.8	0.4	39
Side thruster	2	1	250	280	0.8	0	0	0.8	0.7	289	0.8	0	0
Incinerator	1	1	14	17	0.8	0.2	2.6	0.8	0.2	2.6	0.8	0	0
Workshop	1	1	10	11	0.8	0.2	1.8	0.8	0.2	1.8	0.8	0.2	1.8
Welding equipmt	1	1	32	36	0.8	0.1	2.8	0.8	0.1	2.8	0.8	0.1	2.8
Starting air compr.	2	2	9	10	0.8	0.2	3.1	0.8	0.3	4.9	0.8	0.3	4.9
Control air compr.	1	1	3	4	0.8	0.4	1.1	0.8	0.4	1.1	0.8	0.3	1.1
Air drier	1	1	0.3	0.4	0.8	0.4	0.1	0.8	0.4	0.1	0.8	0.3	0.1
Total							210			535			107

Table 5.2: Hotel power load chart (*Marine Insight, 2020*).

relatively low. For our current methodology we assume that the hotel power amounts to 5% of the installed engine power (cf. *De Vos and Van Gils, 2011*).

$$P_{\text{hotel}} = 0.05 \cdot P_{\text{installed}} \quad (5.25)$$

Combining [Equation 5.24](#) and [Equation 5.25](#) yields:

$$P_{\text{total}} = P_{\text{propulsion}} + P_{\text{hotel}} \quad (5.26)$$

5.1.3 Energy and emission factors

The previous subsections outlined methods to estimate the total resistance a vessel experiences while sailing at a given speed through a waterway, and the total power that is required to achieve this. The next step in the methodology ([Figure 5.2](#)) is to estimate the amount of energy that is involved so that we can make a translation to emissions by using emission factors. This is done in three steps:

1. from total resistance (kN) to total power required (kW),
2. from total power required (kW) and trip duration (Δt) to fuel consumption (kg/kWh), and
3. from fuel consumption (kg/kWh) to emissions (kg) using emission factors.

We will elaborate these steps for diesel fuel.

Step (1)

Making use of [Equation 5.1](#), [Equation 5.17](#) and [Equation 5.26](#) we can estimate the total power requirement as:

$$P_{\text{total}} = P_{\text{hotel}} + \frac{V_s R_T}{\eta_0 \eta_r \eta_h \eta_g \eta_t} \quad (5.27)$$

Step (2)

The fuel consumption to produce this power depends on the vessel (class, engine type, engine age) and the fuel type. The specific energy content of diesel is around 45 MJ/kg , i.e. 12.5 kWh/kg . Not all of this is generated by the engine, due to efficiency losses. The energy production of a diesel engine lies in the range of $4 - 5 \text{ kWh/kg}$ fuel, depending on the age of the engine. This means that the amount of diesel needed to produce the total required power for a trip of duration Δt follows from:

$$W_f \approx \epsilon_d \cdot P_{\text{total}} \cdot \Delta t \quad (5.28)$$

in which W_f is the amount of fuel needed to produce the total amount of power for a trip expressed in kg diesel and the factor $\epsilon_d = 0.20 \div 0.25 \text{ kg diesel/kWh}$.

Step (3)

The total emissions of a gas x for a trip of duration Δt can be derived from (Hulskotte and Bolt, 2012):

$$EM_x = EF_x \cdot P_{\text{total}} \cdot \Delta t \quad (5.29)$$

where EF_x is an emission factor for a compound that is present in the fuel used.

Diesel fuel consists of carbon for 86%, which means that the carbon content of diesel fuel is 720 g/l . Combustion to CO_2 adds 1920 g/l of oxygen, so a litre of burnt diesel fuel produces 2640 g CO_2 . The specific density of diesel fuel is 0.835 kg/l , so this corresponds with $2.640/0.835 = 3.16 \text{ kg CO}_2/\text{kg fuel}$.

This means that on the above trip the total emission amounts to $3.16 \times W_f \text{ kg CO}_2$, or $0.00316 \times W_f \text{ ton CO}_2$. Assuming $\epsilon_d \approx 0.225$, the emission factor for CO_2 is then

$$EF_{\text{CO}_2} = EM_{\text{CO}_2}/(P_{\text{total}} \cdot \Delta t) = 3.16 \cdot 10^{-3} W_f / (W_f / \epsilon_d) \approx 7 \cdot 10^{-4} \text{ ton CO}_2/\text{kWh} \quad (5.30)$$

Note that this refers to energy produced by the engine, not the total energy content of the fuel. Once the total emissions of gas x for a trip of duration Δt are known, they can be translated to emissions per unit time, per unit distance or per unit cargo to assess network performance.

5.1.4 Emission rates: CO_2 , PM10 and NO_x

The previous subsection showed the basic steps involved to go from energy consumption to emissions. For the final step in our methodology (Figure 5.2) it is important to realise that the emission factor, EF_x , is not a constant.

First, it makes a difference what the age of the engine is. Second, the engine usage makes a difference. Segers (2021) addresses the first issue by picking a general emission factor (EF_{general}) from a table, and the second one by implementing a correction factor ($C_{\text{correction}}$) that is related to engine usage:

$$EF_x = EF_{\text{general}} \cdot C_{\text{correction}} \quad (5.31)$$

The x in EF_x can refer to different emission types (e.g CO_2 , PM10 and NO_x).

Engine age

The construction year of the engine is likely to affect the general emission factor. Over the years the preference changed from slow to fast running engines. Furthermore, ongoing technological development has resulted in changes in the emission patterns.

Table 5.3 lists data provided by TNO (Ligterink et al., 2019) regarding general emission factors. For each ‘engine construction year’-class, a specific fuel consumption is specified, and corresponding general emission factors for CO₂, PM10 and NO_x are given.

Construction year classes	Weight class	Fuel consumption [g/kWh]	CO ₂ [g/kWh]	PM10 [g/kWh]	NO _x [g/kWh]
1900 - 1974	L1 – L3	235	746	0.6	10.8
1975 - 1979	L1 – L3	230	730	0.6	10.6
1980 - 1984	L1 – L3	225	714	0.6	10.4
1985 - 1989	L1 – L3	220	698	0.5	10.1
1990 - 1994	L1 – L3	220	698	0.4	10.1
1995 - 2002	L1 – L3	205	650	0.3	9.4
2003 - 2007 CCR-1	L1 – L3	200	635	0.3	9.2
2008 - 2018 CCR-2	L1 – L3	200	635	0.2	7
2019 - 2019 CCR-2	L2 – L3	200	635	0.2	7
2019 - 20xx stage V	L1	205	650	0.1	2.9
2020 - 20xx stage V	L2 and L3	190	603	0.015	2.4

Table 5.3: General emission factors of CO₂, PM10 and NO_x for different construction year classes of marine engines (Ligterink et al., 2019).

By providing a ‘construction year class’ as input, an emission estimation algorithm can pick the appropriate specific fuel consumption and general emission factors from the table.

Partial engine load

Emissions are different in each of the four stages of motion a vessel experiences, viz. stationary, accelerating, steady propulsion and decelerating:

- in the steady propulsion stage a vessels sails at its average operational speed, which is different for every vessel class and for loaded and unloaded sailing;
- in the stationary and deceleration stages, experience shows that the engine takes only about 15% of its maximum power; while
- in the acceleration stage the vessel uses its maximum power.

Engines are less efficient when the partial engine load is low. This results in higher emission factors; more incomplete combustion processes result in higher emission.

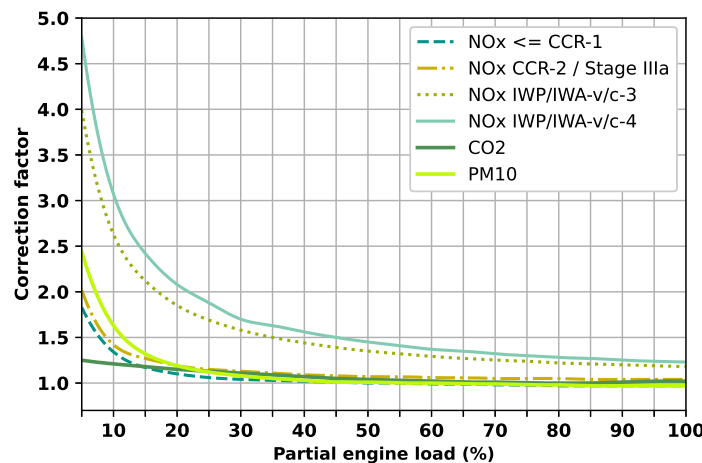


Figure 5.8: Partial engine load factors based on the values from Ligterink et al. (2019) (image modified from Segers, 2021, by TU Delft – Ports and Waterways is licenced under CC BY-NC-SA 4.0).

To take this effect into account, the general emission factor (see Table 5.3) has to be multiplied by a correction factor (see Figure 5.8) that reflects the additional emission due to partial engine load.

Selecting the appropriate general emission factors based on engine age, and subsequently applying a correction factor related to engine load, accounts for the largest effects that influence the correction factor. With this, our methodology to estimate energy consumption and emissions is complete.

5.1.5 Composite results

In this subsection we show some examples of the behaviour that results from an algorithm that includes all aspects mentioned.

Emissions as a function of vessel speed

As a first example we inspect how the emissions of an M9 vessel, with a given engine age (viz. 1990) and dimensions ($L_s = 135m$, $B_s = 11.45m$, $D_s = 2.75m$), behave as a function of vessel speed on the one hand, and water depth on the other. Figure 5.9 shows the results from applying the algorithm. NB: the emissions are expressed in g/km .

For very low vessel speeds, the engine is not used in its optimal range. Figure 5.8 shows that for lower partial engine loads the correction factor increases dramatically. Furthermore, due to low vessel speeds, the vessel takes longer time to travel a certain distance and thus accumulates more emissions during that certain distance, which in turn results in a strong increase in the emissions in g/km .

For very high speeds, the resistance will greatly increase. Figure 5.4 illustrates how the wave related resistance in particular, will increase drastically. So even though higher velocities mean that the emissions will be spread out over a larger area, the cumulative effect still results in a strong increase in the emissions in g/km .

On top of these two aspects Figure 5.9 clearly shows the sensitivity of the emissions in g/km to reduced water depths.

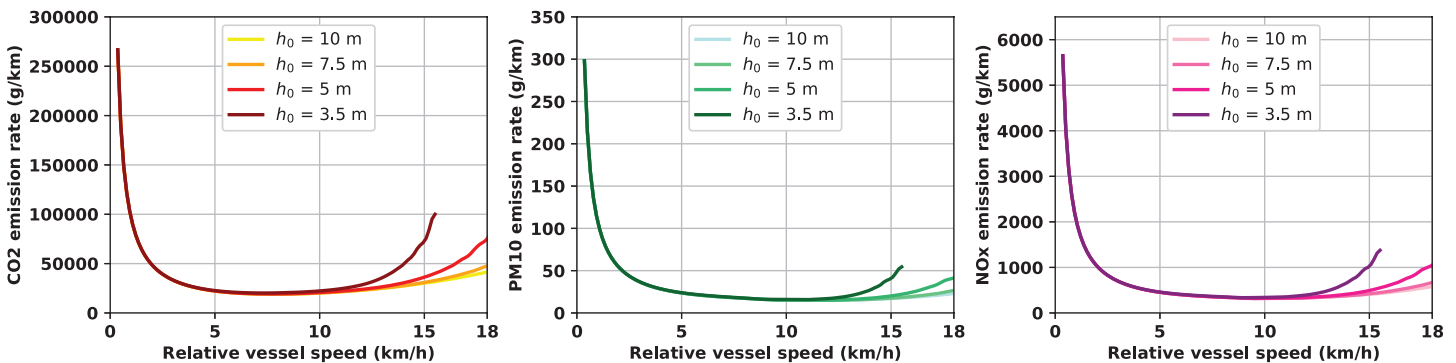


Figure 5.9: Emissions as a function of vessel speed (images modified from Segers, 2021, by TU Delft – Ports and Waterways are licenced under CC BY-NC-SA 4.0).

Emissions as a function of partial engine load

As a second example we inspect how the emissions of an M9 vessel, with given dimensions ($L_s = 135m$, $B_s = 11.45m$, $D_s = 2.75m$) and for a given water depth (viz. $h_0 = 10m$), behave as a function of vessel speed on the one hand, and engine age on the other. Figure 5.10 shows the results from applying the algorithm. NB: the emissions have again been expressed in terms of g/km .

The effect of newer engine ages is clearly visible in the emission rates. Especially for the nitrogen oxides (NO_x) and particulate matter (PM10) a significant difference in the emission rates between older and newer engines can be observed. For PM10, the emission rates drop nearly down to zero for the newest engines.

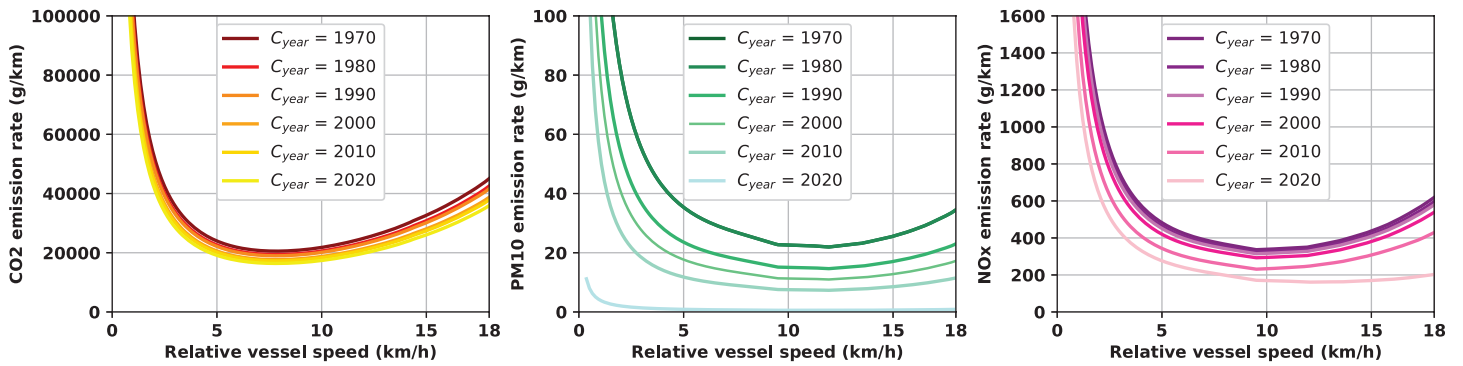


Figure 5.10: Emissions as a function of engine age (images modified from Segers, 2021, by TU Delft – Ports and Waterways are licenced under CC BY-NC-SA 4.0).

In summary the following parameters have the largest influence on the emission rates of IWT-vessels. Changes in the amount of installed power particularly affect the particulate matter (PM10) emission rates. Changes in vessel speed have the largest effect on CO₂ emission rates. Changes in the engine age have a significant influence on the nitrogen oxides (NO_x) and particulate matter (PM10) emission rates. Technological innovation has already reduced CO₂ emission rates, so that emission type is less sensitive for engine age. The next section shows how the methodology described above (see Figure 5.2) can be used to analyse network performance.

5.2 Emission performance of transport corridors

The previous section described a methodology to estimate the energy consumption and associated emissions of an IWT-vessel. The trigger for its development came from emission reduction objectives that followed from the global Paris Agreement and the subsequent more local implementations of it via Green Deals and IMO regulations.

In *Frame of Reference (FoR)* terms the reduction targets from the *Green Deal (2019)* can be regarded as operational objectives. The methodology from *Section 5.1* can be regarded as a *Quantitative State Concept (QSC)* that helps to quantify these operational objectives. A logical next step is to apply the methodology to assess network performance. As outlined in *Part I – Section 2.2.2* and *Chapter 1* of the current Part this requires the definition of indicators, defined as assemblages of QSCs that indicate whether or not there is a problem. In this section we will show how the methodology for energy consumption and emission estimation can be used to investigate the emission performance of a corridor.

5.2.1 Analysis of a single trip

To analyse vessel performance on a network, some basic information should be available that can typically be found in vessel trip logs. *Table 5.4* shows the first few lines of a vessel trip log and some basic information it may contain on position and time. In this case each row represents an incremental move event of a vessel. In other cases a log can take the form of a list of consecutive positions and timestamps, but the information is the same.

The first two columns in *Table 5.4* indicate the start and stop time of the move, and the second two columns the corresponding geographical coordinates. As indicated underneath the table this information can be used to derive the travelled distance, Δx , and the travel time, Δt . With this the average vessel speed, V_s , during the move event can be derived. Assuming we know the vessel dimensions (L_s , B_s and D_s) and the average waterway characteristics (h_0 and U_c) at the location where the move event took place, we have all the information needed to estimate the total resistance (kN) the vessel experiences and the total energy (kWh) that was consumed during the move event. When, furthermore, we know (or assume) the engine age and the average partial load, we can estimate the total potential emissions of CO₂, PM10 and NO_x that occurred during the move event (see *Figure 5.2*). By repeating this procedure for each move event in the trip log a vessel's energy consumption and potential emissions can be estimated as a function of space and time.

	time_start	time_stop	edge_start	edge_stop	total_energy	total_emission_CO2	total_emission_PM10	total_emission_NOX
0	2020-09-26 00:00:00.000000	2020-09-26 00:01:37.988698	POINT (4.40878376619477 51.6893044653478)	POINT (4.407711423268813 51.68872877120878)	1.028666	797.232566	0.379078	11.358754
1	2020-09-26 00:01:37.988698	2020-09-26 00:01:46.039699	POINT (4.407711423268813 51.68872877120878)	POINT (4.407623317192122 51.68868147089958)	0.084518	65.502657	0.031146	0.933264
2	2020-09-26 00:01:46.039699	2020-09-26 00:04:00.501781	POINT (4.407623317192122 51.68868147089958)	POINT (4.40615183993005 51.6878914989466)	1.411557	1093.978722	0.520178	15.586713
3	2020-09-26 00:04:00.501781	2020-09-26 00:23:56.405478	POINT (4.40615183993005 51.6878914989466)	POINT (4.3925552967856 51.6812504548851)	12.554364	9729.829984	4.626459	138.627991
4	2020-09-26 00:23:56.405478	2020-09-26 00:24:52.273815	POINT (4.3925552967856 51.6812504548851)	POINT (4.39198470467551 51.6808950327794)	0.586495	454.542805	0.216132	6.476203

$$V_s = \Delta x / \Delta t \rightarrow P_{\text{tot}} \rightarrow E_{\text{tot}} \rightarrow \text{Emissions}$$

Table 5.4: Vessel log: input for energy consumption and emission calculations (table by Segers, 2021, is licenced under CC BY-NC-SA 4.0).

It is good to realise that an actual trip log, in terms of information on position and time, does not differ too much from a simulated trip log. This means that the methodology can be applied to both measured and simulation trip log data. NB: there will be some differences in resolution as we will see in the next subsections.

A well-known vessel tracking system is the [Automatic Identification System \(AIS\)](#) that collects specific data that vessels transmit via on-board transceivers and makes it available to waterway users and [Vessel Traffic Service \(VTS\)](#)-operators to promote safe navigation. AIS logs are lists of consecutive positions and timestamps, and often contain additional information such as the [IMO](#) identification number, the ship name, the ship type, the ships basic dimensions, draught, etc. Note that some of the additional information has to be submitted manually, and as a consequence is not very reliable, but position and time are not manual inputs. Rather these are values derived automatically from the ship's [Global Positioning System \(GPS\)](#). As such they are considered quite reliable (even though this data may contain outliers depending on environmental conditions). An alternative source for measured data may be the ship's own on-board logging system.

Simulation models, as described in [Section 2.6](#) (i.e. OpenTNSim, OpenCLSim), also produce vessel trip logs as output. Before the simulation starts, the modeller needs to provide input on vessel dimensions and waterway properties to drive the simulation. As a consequence, the information to apply the methodology described above is also available.

As can be seen in [Table 5.4](#) the energy consumption and emissions can be estimated and added to the log for each move event. These 'enhanced' logs can then be used for analysis. Deriving the trip totals is a simple matter of addition. More interesting is the fact that energy consumption and emissions can now be 'known' in space and time. Network performance can now be analysed by adding the results of all trips for a given day, for example or all emissions on a specific stretch of the network. The next subsection provides examples of this.

5.2.2 Analysis of a representative set of trips

In response to a question by Rijkswaterstaat, [Segers \(2021\)](#) developed the methodology described in [Section 5.1](#). To analyse its performance she applied the methodology to the busiest part of the Dutch [IWT](#) network: the Rotterdam–Antwerp corridor (see [Figure 5.11](#)).

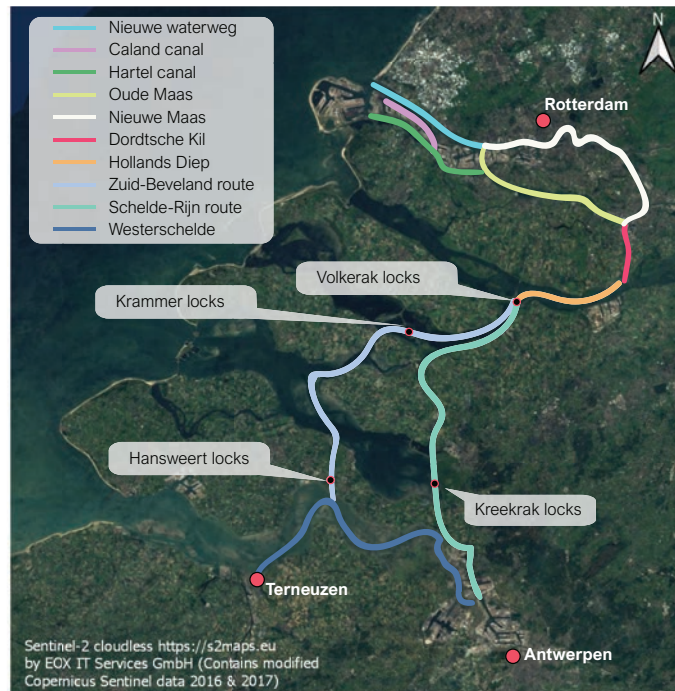


Figure 5.11: The Rotterdam-Antwerp corridor (image modified from Segers, 2021, by TU Delft – Ports and Waterways is licenced under CC BY-NC-SA 4.0).

AIS data

A starting point for the analysis of Rotterdam-Antwerp corridor emissions, based on AIS data, is to first look at the traffic intensity. Figure 5.12 shows the number of vessels counted on the network’s key waterway sections, for September 2nd, 2019.



Figure 5.12: Traffic intensity as derived from AIS for the Rotterdam-Antwerp corridor for September 2nd, 2019 (image modified from Segers, 2021, by TU Delft – Ports and Waterways is licenced under CC BY-NC-SA 4.0).

Figure 5.13 shows the resulting heatmaps for CO_2 , PM_{10} and NO_x , for September 2nd, 2019, based on individual vessel trips. NB: the figures show the cumulative emission ‘potentials’ for IWT-vessels for a specific day.

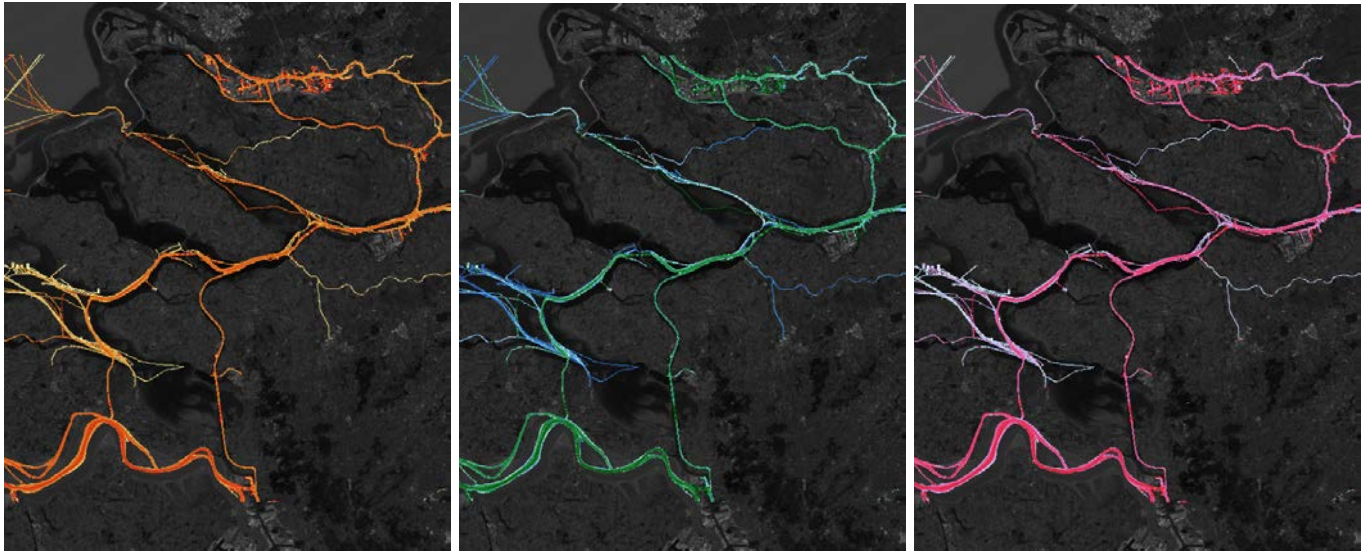


Figure 5.13: Heatmaps for potential CO_2 , PM_{10} and NO_x emissions, for September 2nd, 2019, based on AIS data directly (images by Segers, 2021, are licenced under CC BY-NC-SA 4.0).

Despite the fact that the subfigures in Figure 5.13 look interesting at first glance, there are limitations to their practical use. Ideally one would want to aggregate the emission heatmaps and attribute the summed emissions to the specific elements of the transport graph. Figure 5.14 shows that (potential) emissions are not uniformly distributed over the network. Rather there are areas with higher emission potentials (corresponding with the busier parts of the network) i.e. apparent emission potential hotspots. These hotspots are associated with the presence of locks (see Figure 5.11). At these locations vessels sail slowly, or lie stationary for a period of time. Lower vessel speeds mean less energy consumption per unit time, so lower emissions. This reduction, however, is counter balanced by lower partial engine loads, which in turn increases emissions. When the vessels lie still, e.g. in the lock waiting area or during levelling, the engine is idling and only hotel power is used. While in such cases the emissions per unit time may be low, emissions per unit space will increase due to local accumulation.

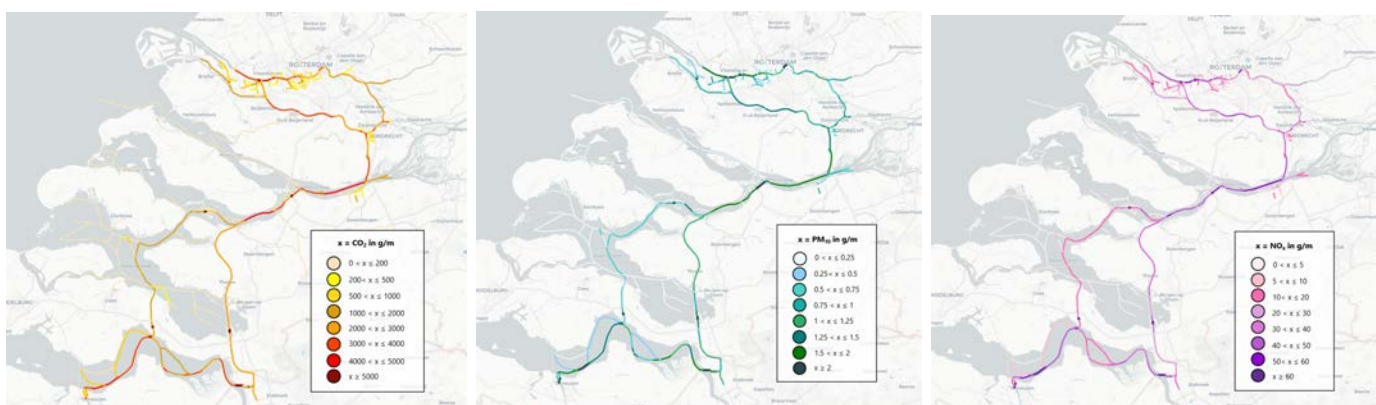


Figure 5.14: Potential CO_2 , PM_{10} and NO_x emissions, for September 2nd, 2019, based on AIS data, projected on the transport network (images by Segers, 2021, are licenced under CC BY-NC-SA 4.0).

OpenTNSim simulation data

Now that we have the basic information on potential emissions based on AIS data, a next step is to simulate a similar traffic pattern using OpenTNSim. For this, Segers (2021) analysed the AIS data to create an Origin-Destination matrix based on the data of September 2nd, 2019. By running a simulation for the same date, using

the Origin-Destination matrix, averaged vessel speeds and an assumed distribution of engine ages in the fleet as input, a quite encouraging match between the two results can be found (see Figure 5.15).

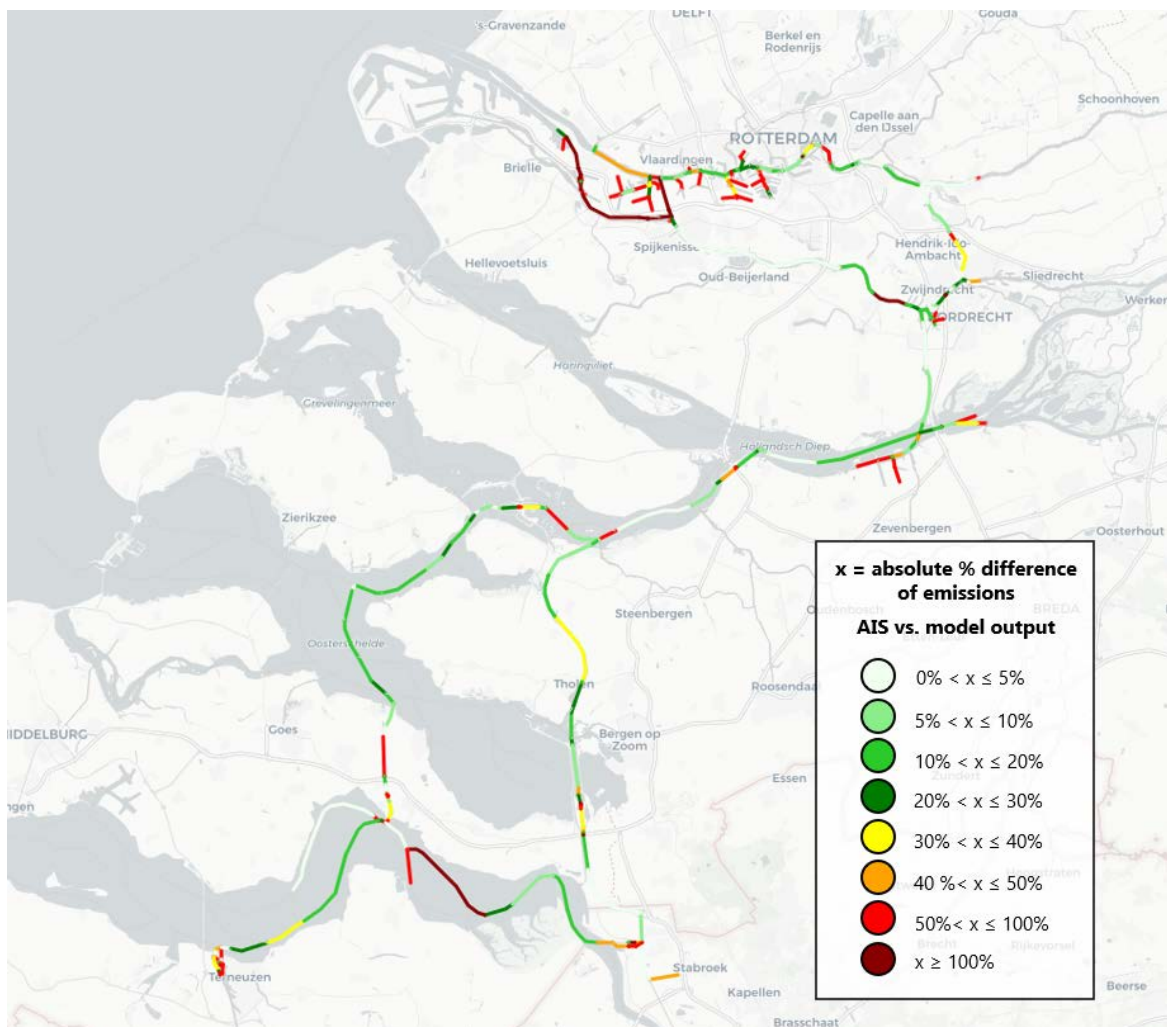


Figure 5.15: Comparison of the results based on AIS data with the results derived from OpenTNSim simulations (image by Segers, 2021, is licenced under CC BY-NC-SA 4.0).

Obviously there are still differences between the ‘measured’ and ‘modelled’ results, but by and large differences are smaller than 20% and for large stretches of the network even smaller than 10%. The main cause of these differences, for now, is that the AIS data provides a lot of detail on accelerations and decelerations over the network, while the simulation uses an averaged speed for the entire trip from origin to destination. Since the effect of sailing speed on frictional resistance responds quadratically (see Equation 5.2) and additional effects can be expected in shallower water, these differences between average and actual speed may lead to significant local differences. But the comparison is encouraging nonetheless. The analysis also allows us to inspect estimated totals, which shows a similar result (see Table 5.5).

	AIS t0 emission scenario	Model simulation t0	Difference
Average fuel consumption [L/h]	110	119	8.2%
Average required power [kW]	446	482	8.1%
Total fuel consumption [L]	545,868	530,730	-2.8%
Total CO ₂ emission [kg]	1,551,610	1,547,533	-0.3%
Total PM10 emission [kg]	712.61	685.86	-3.8%
Total NO _x emission [kg]	19,966	19,546	-2.1%

Table 5.5: Output of AIS ‘t0 emission scenario’, compared to model simulation output: Average fuel consumption and power; Total fuel consumption and potential emissions of one day (2 Sept 2019) (Segers, 2021).

Next to the relative differences between ‘measured’ and ‘modelled’ results, it is also good to note that there will be differences between theory and practice in terms of the absolute numbers. The AIS data was filtered to only include cargo vessels and assumptions were made about installed power and engine age. Furthermore, assumptions were made on water depths, based on a combination of highly detailed bed information with much coarser water level information. Next, we know that parts of the Rotterdam-Antwerp corridor experience currents, either of river discharge origin, or tidal origin. While currents can straightforwardly be incorporated in the methodology, actually acquiring this information for all parts of the network as a function of time can be quite a challenge. For this reason this aspect was not yet included by (Segers, 2021) and is further research is recommended.

Comparison of measures

The ability to estimate a t_0 state based on AIS data is an encouraging step forward en route to the development of energy consumption and emission-related network performance indicators. A next step would be to define time intervals and traffic patterns to determine a desired or reference state.

Another encouraging result is that there is a reasonable agreement between the measured and simulated t_0 , certainly in terms of averages. This allows policy analysts to test and compare various emission reduction packages.

(Segers, 2021) showed how this could work for a number of measures, viz. an engine renewal policy and sailing speed limitations. (Vehmeijer, 2019), using a slightly different quantification method, looked at the potential effects of modifying the network with higher bridges or the conversion of a sluice to a lock, both interventions influence the sailing distance and emissions.

5.3 Multi-modal corridor analysis

Section 5.1 describes how to quantify one specific aspect of transport over water, i.c. the energy consumption and associated emission patterns of IWT vessels. Section 5.2 shows how to extrapolate this to fleet performance on a given corridor, and to the assessment of alternative emission-reducing measures. A next level of complexity is to study the multi-modal performance of corridors.

5.3.1 A case study: Myanmar

A private developer intends to develop an industrial estate along the Ayeyarwady River near Mandalay City, about 900km upstream from Yangon, the main sea port in Myanmar. IWT over the Ayeyarwady River has traditionally been the preferred mode of transport in Myanmar, from ancient times to more recent years. In the first decades of the 20th century, the Irrawaddy Flotilla Company (IFC) was the largest IWT company in the world, owning over 600 vessels carrying more than 6 million passengers and more than 1 million ton of cargo. More recently however, investments in roads have improved transport by truck and cars. Passenger traffic by boat has declined and long-distance passenger travel has totally disappeared. The basic questions to be answered are:

- which types of cargo can be attracted by the river port,
- what volumes of cargo can be attracted by the river port, and
- at what tariff can the goods be handled at the port, providing a profitable business whilst remaining a competitive mode of transport?

Step 1: Market Study - Trade flows. Demand and Supply

As a first step of the studies (RHDHV, 2015), Origin - Destination matrices were compiled, showing what types of cargo at what volumes are currently transported from/to the wider Mandalay Region (Figure 5.16). The cargoes were split into main commodities, e.g. various dry bulk, agricultural and timber products. The volumes are based on interviews or surveys with existing cargo transporters and available country statistics. Future volumes of cargo are based on economic forecasts and information of major (industrial) developments taking place in the region, e.g. in the mining sectors, industrial estates and general trends in developing economies.

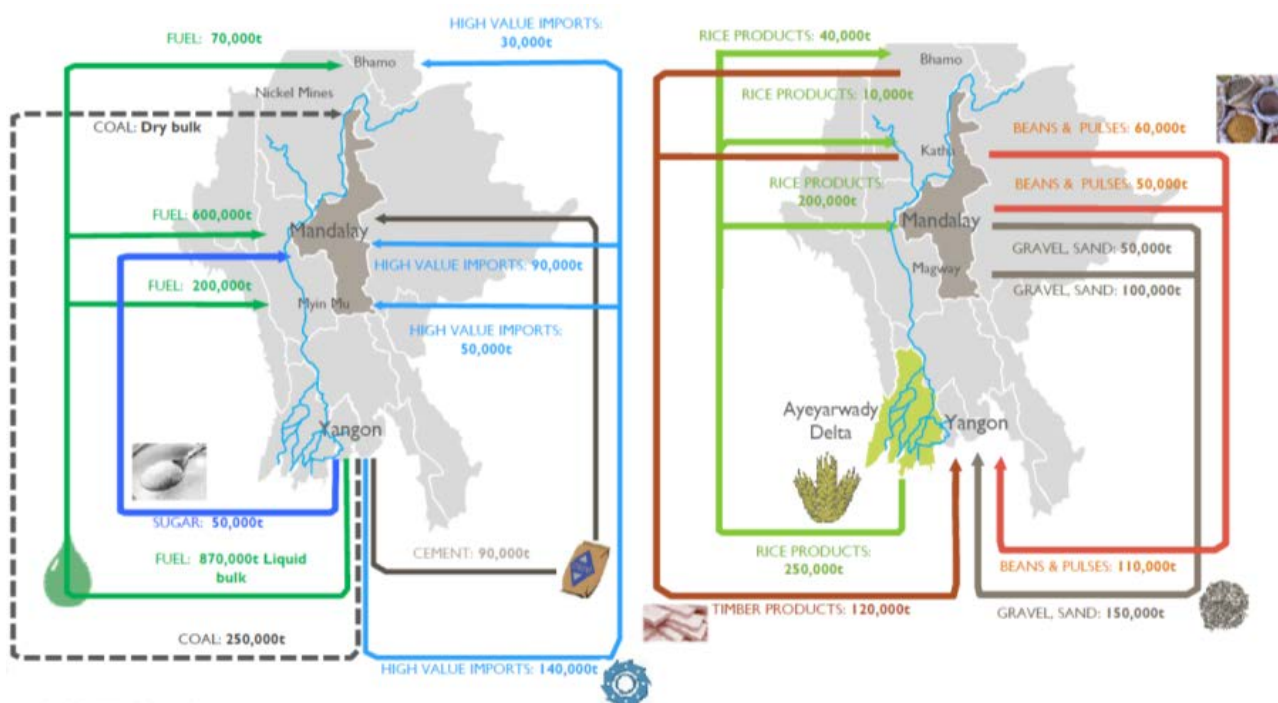


Figure 5.16: Analysis of origins and destinations for various types of cargo (for illustrative purposes only) (by Royal HaskoningDHV is licensed under CC BY-NC-SA 4.0).

Table 5.6 presents the cargo currently transported by river transport from/to various cities along the Ayeyarwady River. A river port near Mandalay would be able to capture cargo destined for or originating from Mandalay, but also provide transshipment services for cargo from/to upstream ports using smaller (500t) vessels.

RIVER PORT THROUGHPUT (TONNE/ANNUM)											
Name	Irrawaddy										Total
	Yangon	Delta	Magway	Nyaung U	Pakokku	Myin Mu	Mandalay	Katha	Mines	Bhamo	
Vessel size (DWT)	1,000	1,000	1,000	1,000	1,000	1,000	1,000	500	500	500	
Import	450,000	0	30,000	70,000	30,000	170,000	1,020,000	40,000	250,000	130,000	2,180,000
Export	1,350,000	280,000	30,000	20,000	40,000	10,000	210,000	30,000	20,000	120,000	2,180,000
Annual Throughput	1,800,000	250,000	50,000	80,000	50,000	190,000	1,180,000	130,000	270,000	250,000	4,370,000

Table 5.6: Cargo transported by river transport from/to various cities along the Ayeyarwady River (for illustrative purposes only) (by Royal HaskoningDHV is licensed under CC BY-NC-SA 4.0).

In addition to the existing cargo flows over the river, it was recognized that new businesses on the industrial estate will attract large volumes of cargo. The demand for fuel products in central and northern Myanmar has risen sharply over the last decade and therefore fuel storage shows good potential. Several private developers have shown interest in collaboration to develop such a storage facility within the port. This may attract considerable cargoes.

Step 2: Mapping of available transport corridors & modes of transport

The existing and future cargo flows can be transported by barge, rail and road. Liquid bulk (oil products) can be transported by pipeline. All available transport means from the main origins and destinations where mapped (see Figure 5.17), including travel distances and any development which may take place in the coming years and decades, such as road improvement, river improvement projects or railway extensions.

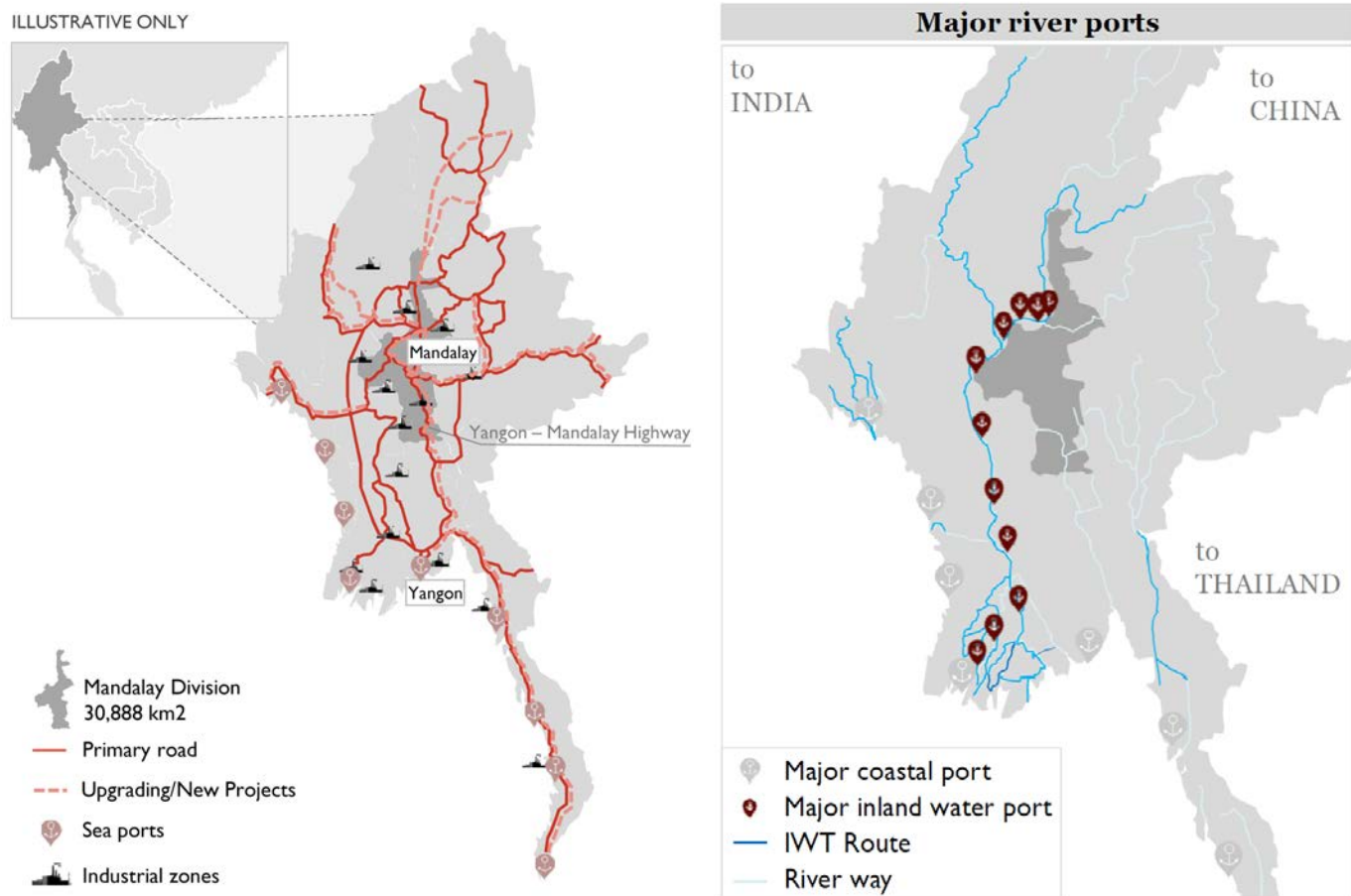


Figure 5.17: Analysis of origins and destinations for various types of cargo (for illustrative purposes only) (by Royal HaskoningDHV is licensed under CC BY-NC-SA 4.0).

Step 3: Intermodal competition

When cargo owners decide to ship cargo to a given destination, they will have to decide which mode of transport to use based on a) costs, b) time and c) reliability. Some examples of how these three factors can influence their choice are:

- Agricultural goods are perishable. Fast transport is required. This is more evident for fruits than for dried products, such as rice or dried beans. The value of the product will decrease with time, hence transport costs can be higher, provided goods will be delivered more quickly.
- Demand for cement for the construction industry is relatively predictable and may depend on planned projects. Delivery within foreseeable time and having some storage allows the choice for lowest-cost mode of transport.
- Containers need to be fully loaded to achieve optimum efficiency. Many small transport companies in developing countries, often with individual truck owners, prefer small trucks over container transport. Fuel subsidies makes trucking more competitive than barging for which no such subsidy scheme exists.

To calculate the costs per tonne for each mode of transport, surveys with transport companies have been carried out. Costs are expressed in USD/t or TEU/t for containers (see Table 5.7).

To gain a precise insight in total transportation costs between origin and destination, it may well be that cargo changes modes of transport. This is for instance applicable to container transport which requires loading and offloading in a port onto trucks before it can be delivered to the final destination. In some cases, the container is emptied in a warehouse from where individual cargoes are transported further. It is therefore important to gain insight into the complete corridor of transport rather than the individual legs.

Mandalay to Yangon Comparison	 ROAD	 RAIL	 RIVER
Cost \$/t (Min)	\$50	\$54	\$32
Cost cents/t/km	7.1c	8.7c	3.5c
Distance (km)	705	617	917
Timing (days)	2	4	7
Capacity	<ul style="list-style-type: none"> ▪ Cargo trucks/break bulk: 15-27 tonnes (12 wheelers) ▪ Oil tankers/Liquid bulk: 3 kinds: 2,800 gal; 5,200 gal; 7,000 gal 	<ul style="list-style-type: none"> ▪ 1,500 horsepower: 15 freight cars, each car taking max. 30 tonnes or 15 containers ▪ 2,500 horsepower: 30 freight cars, each car taking max. 30 tonnes or 30 containers 	<ul style="list-style-type: none"> ▪ Cargo Barges (200 x 50ft.) <ul style="list-style-type: none"> - Tonnage (DWT): 600t-Dry, 1000t-Wet (Max: 1000-1200) - Containers (20ft.): 1 "level": 42 containers 2 "levels": 60-80 containers (Max) - Draft (when loaded): 1.4 m ▪ Oil Barges: <ul style="list-style-type: none"> - Gallons (US gl.): 280,000 (in dry), 350,000 (in wet) ▪ Land Craft Transporters <ul style="list-style-type: none"> - Tonnage (DWT): 600t-Dry, 1000t-Wet (Max: 1000-1200) - Vehicles: tractors and heavy machinery and equipment
Advantages / disadvantages	<ul style="list-style-type: none"> ▪ Road is direct, fast and necessary per shipment ▪ Road has a wide network ▪ High cost, low volume per shipment 	<ul style="list-style-type: none"> ▪ Rail is larger volume per shipment ▪ Rail network is less direct ▪ Cost is high due to excessive handling 	<ul style="list-style-type: none"> ▪ Lowest cost per tonne by far ▪ River is by far the largest volume per shipment ▪ Has the least direct network

Table 5.7: Comparison of different modalities to transport cargo between Mandalay and Yangon along the Ayeyarwady River (for illustrative purposes only) (by Royal HaskoningDHV is licensed under CC BY-NC-SA 4.0).

Since the improvement of roads in Myanmar, larger trucks were able to travel larger distances much faster. The time to deliver goods from Mandalay to Yangon currently requires 2 days by truck, whereas rail would take 4 days and by river transport 7 days.

The reliability of transport is often expressed as the variation in travel time. Congestion on roads can increase the road travel time considerably, sometime heavily influenced by weather conditions and poor road maintenance. Rail is often reliable as there is a fixed schedule, but delays as a result of train failure or track repairs can be substantial. River transport experiences delays during the dry season, where some shallow sections on the river cannot be used for several days.

Shippers factor this into their price as well, hence dry season transport is more expensive than wet season transport. Investments into river transport improvements are often dedicated to removing bottlenecks, to increase the reliability of this mode of transport.

Figure 5.18 presents the transportation time of goods from the origin to destination, in which all steps are defined in terms of time and costs (USD/t).

Step 4: Market Share and Capacity River Port

Based on the regional market forecast for the cargo and the distribution of cargoes between various modes of transport, a cargo volume forecast that can be attracted by the new river port was made (Figure 5.19). For each cargo, the costs, time and reliability were mapped. A relative share of cargo to each mode was made, based on the preferences expressed by cargo owners, through surveys. Especially liquid bulk cargo and other cargoes proved to be most attractive. Those producing high-value goods which are usually transported by container would prefer trucking, and hence the total share will be relatively low.

Step 5: Tariff study and business case

As a final step, the cost advantage of using the river port over other modes of transport, in combination with the estimated running costs (also expressed in USD/t) of such a port, are used to determine the fee that can be charged to the shipping companies (Figure 5.20). A positive business-case is found once both shipping companies and river port operator have sufficient margins. Very high fees for using the river port can divert cargo from river transport to roads or rail. Very low fees will result in an unprofitable river port which will not be financially sustainable. It may therefore be concluded that before a successful (river) port project will be financed and constructed, a good insight into the transport economics, logistics and port capacity is required. In the below example, a potential port fee of 8 USD/t is calculated. This means that to remain competitive, a port fee of maximum 8 USD/t can be charged. The port fee should be sufficient to cover the costs of constructing and running the proposed river port to the required capacity.

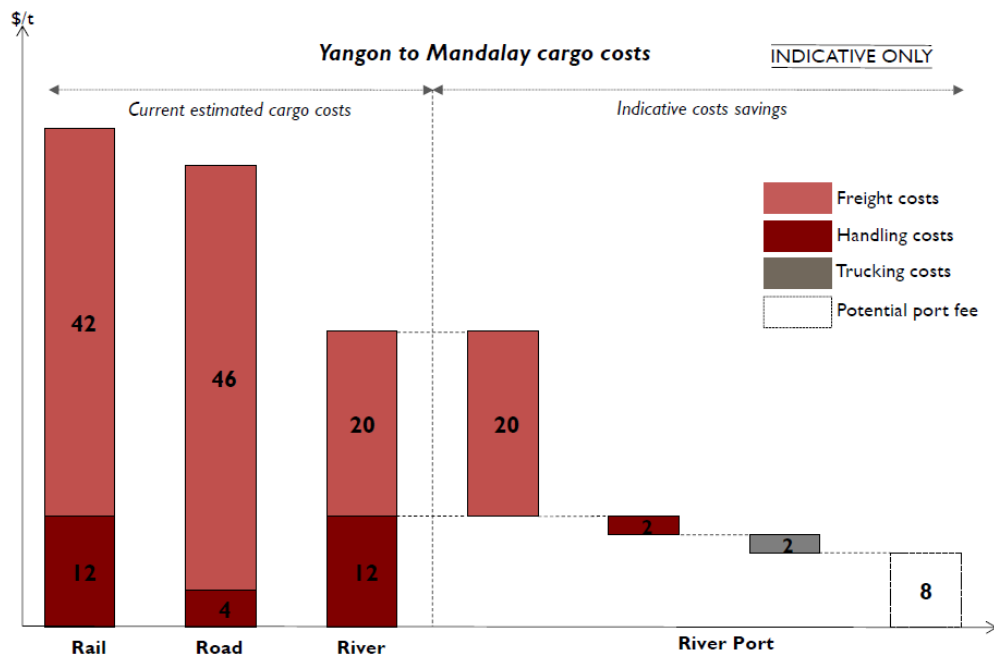


Figure 5.20: Cost comparison of alternatives and potential fee (for illustrative purposes only) (by Royal HaskoningDHV is licensed under CC BY-NC-SA 4.0).

5.4 Concluding

Section 5.3 describes an example of a multi-modal corridor analysis. It is interesting to see how all elements in this book play a role there. To fully grasp the complexity of a corridor, you need to understand current and future demand, the current and future modality mix (including the vessel mix) and the status of the network of ports/terminals and waterways. To investigate multiple potential system configurations, simulation is crucial.